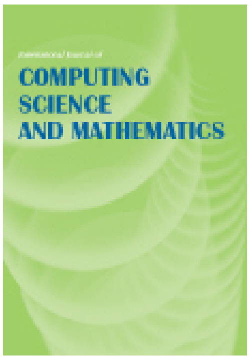

International Journal of Computing Science and Mathematics

ISSN online: 1752-5063 - ISSN print: 1752-5055
https://www.inderscience.com/ijcsm

Research on bonding damage of composite materials adhesive structures

JiaRu Shao, Niu Liu, ZiJun Zheng

DOI: 10.1504/IJCSM.2024.10062421

Article History:

Received:	27 July 2021
Last revised:	10 April 2023
Accepted:	05 May 2023
Published online:	22 February 2024

Research on bonding damage of composite materials adhesive structures

JiaRu Shao, Niu Liu* and ZiJun Zheng

College of Mechanical Engineering,
Chongqing University of Technology,
Chongqing, Chongqing, 400000, China
Email: shaojiaru@cqut.edu.cn
Email: ln19970509@2015.cqut.edu.cn
Email: zhengzj@cqut.edu.cn
*Corresponding author

Abstract: In this paper, continuum damage mechanics (CDM) and the 3D Hashin criterion are implemented to simulate the formation and evolution of the intra-laminar damage. The cohesive layer was simulated by the cohesive zone model (CZM). The finite element method (FEM) results are consistent with the experimental results, which validate the effectiveness of the FEM. Then, different types of adhesively bonded single-lap joints (SLJs) are analysed. The results suggest that the 0° and 90° plies can improve the failure loads of SLJs. The ±45° plies are beneficial for alleviating the damage to the adhesive layer. The increase in overlap width has less influence on the damage location and damage modes. Matrix damage and delamination, with less fibre damage, are the main damage modes of SLJs with lower adherend thickness. With the thickness of the adherend increasing, matrix damage and delamination take up an increasingly smaller proportion.

Keywords: composite materials; adhesive connection; fibre damage; matrix damage; adhesive damage; finite element method.

Reference to this paper should be made as follows: Shao, J., Liu, N. and Zheng, Z. (2024) 'Research on bonding damage of composite materials adhesive structures', *Int. J. Computing Science and Mathematics*, Vol. 19, No. 1, pp.39–52.

Biographical notes: JiaRu Shao is a Professor at the College of Mechanical Engineering, Chongqing University of Technology. His main research fields are aerospace equipment design, machine vision and SPH. He has been involved in several National Science and Technology Major Projects in China and has achieved many satisfactory research results.

Niu Liu is a postgraduate student at the College of Mechanical Engineering, Chongqing University of Technology. His main research fields are the mechanism of composite materials and aerospace equipment design.

ZiJun Zheng is a Professor at the College of Mechanical Engineering, Chongqing University of Technology. His main research fields are computational mechanism, mechanism of composite materials and metal plastic forming. He has participated in a number of researches on technology and scheme design of aircraft, and has extensive experience in this field.

1 Introduction

Composite materials have been wildly used in engineering because of their high specific strength, high specific modulus and small specific gravity (Daggumati et al., 2020; Meng et al., 2020). The adhesive bonding cannot only connect the composite components together without affecting the strength of the composite laminates, but also decrease the overall weight of the joints. Therefore, it is of great significance to study the joint strength and damage modes of the single-lap joints (SLJs) and to explore the failure mechanism of SLJs (Sun et al., 2019; Orefice et al., 2018).

Many studies have carried out numerous experimental studies on the adhesive joints. Cheng et al. (2019) conducted a double cantilever beam (DCB) and end notched flexure (ENF) test. Barroso et al. (2020) determined the failure location of the adhesive connection. Yuan et al. (2019) performed ultrasonic high-frequency vibration pretreatment on the surface of the adhesive joint of the composite material. Floros and Tserpes (2019) conducted mode I fracture toughness tests, mode II fracture toughness test and mode II mixed fracture toughness test. Demirala and Kadioglu (2018) conducted tensile experiments on four different stacking sequences of the SLJs, including $[\pm 10°]_{5S}$, $[\pm 20°]_{5S}$, $[\pm 45°]_{5S}$ and $[\pm 55°]_{5S}$. Kupski et al. (2019) conducted tensile tests on four different stacking sequences of the SLJs. Akderya et al. (2016) tested the tensile properties of SLJs under three environmental conditions of –18°C, 25°C and 70°C.

The experiment can obtain more intuitive results, however, the experiment itself is usually time-consuming and costly. In contrast, FEM cannot only observe the damage of the adhesive layer at any time, but also obtain the overall stress change of the adhesive joint. Ungureanu et al. (2018) conducted experiments and FEM analysis on GFRP adhesive joints. The numerical analysis results are in good agreement with the experimental results. Amiri and Farahani (2020) studied the influence of the geometric parameters of button-shaped adhesive joints through finite element analysis. Felger et al. (2019) established a numerical model for predicting the strength of the adhesive layer using the method of stress and energy coupling. Ribeiro et al. (2016) studied the stress distribution of carbon-epoxy composite-aluminium adhesive joints with different overlap lengths through FEM. Cricrì and Perrella (2017) studied the pure type III fracture toughness of composite joints through experiments and numerical analysis. It is found that for practical applications, the influence of fibre orientation on the type III fracture behaviour of adhesive joints is negligible. Kim and Hong (2018) proposed a type I+II mixed damage model based on the B-K criterion based on exponential damage evolution. Masmanidis and Philippidis (2015) proposed a continuous damage model for simulating damage propagation in bonded joints. The numerical analysis results obtained by this model with different overlap lengths are very consistent with the experimental results.

Most of the above studies have focused on the macroscopic connection strength of composite joints. However, few researches have studied the microscopic mechanical behaviour changes and damage modes of SLJs. In this paper, FEM based CDM is used to analyse the tensile performance of SLJs with four dimensional parameters, including different stacking sequences, overlap lengths, overlap widths and adherend thicknesses. The macroscopic connection strength and microscopic mechanical behaviour changes of the SLJs are revealed. The results of this paper have guiding significance for the design of the SLJs and provides a new idea and method for research of the adhesively bonded components.

2 Numerical simulation methodology

Numerical analysis cannot only obtain the connection performance of the SLJs, but also explain the failure mechanism of SLJs microscopically. The SLJs is composed of composite laminates and adhesives. Therefore, the damage of SLJs contains two aspects:

1 the intralaminar damage, including the breakage of fibre and matrix;

2 the failure of adhesive layer, which means that the excessive tensile load causes the adhesive layer to lose its bearing capacity.

2.1 Composite laminate intralaminar damage

The intralaminar damage of composite laminates consists of failure initiation criteria and damage evaluation model. In order to judge the failure initiation and failure modes of composite laminates, the three-dimensional (3D) Hashin failure criterion is introduced in this paper (Hashin, 1980; Ye et al., 2018). The corresponding subroutine is written for the numerical analysis.

Fibre tension failure $(\sigma_{11} > 0)$:

$$\left(\frac{\sigma_{11}}{X_T}\right)^2 + \left(\frac{\tau_{12}}{S_{12}}\right)^2 + \left(\frac{\tau_{13}}{S_{13}}\right)^2 \geq 1 \tag{1}$$

Fibre compression failure $(\sigma_{11} < 0)$:

$$\left(\frac{\sigma_{11}}{X_C}\right)^2 \geq 1 \tag{2}$$

Matrix tension failure $(\sigma_{22} > 0)$:

$$\left(\frac{\sigma_{22}}{Y_T}\right)^2 + \left(\frac{\tau_{12}}{S_{12}}\right)^2 + \left(\frac{\tau_{23}}{S_{23}}\right)^2 \geq 1 \tag{3}$$

Matrix tension failure $(\sigma_{22} < 0)$:

$$\left(\frac{\sigma_{22}}{Y_C}\right)^2 + \left(\frac{\tau_{12}}{S_{12}}\right)^2 + \left(\frac{\tau_{23}}{S_{23}}\right)^2 \geq 1 \tag{4}$$

Fibre-Matrix shear out $(\sigma_{11} < 0)$:

$$\left(\frac{\sigma_{11}}{X_C}\right)^2 + \left(\frac{\tau_{12}}{S_{12}}\right)^2 + \left(\frac{\tau_{23}}{S_{23}}\right)^2 \geq 1 \tag{5}$$

Delamination in tension $(\sigma_{33} > 0)$:

$$\left(\frac{\sigma_{33}}{Z_T}\right)^2 + \left(\frac{\tau_{23}}{S_{23}}\right)^2 + \left(\frac{\tau_{13}}{S_{13}}\right)^2 \geq 1 \tag{6}$$

Delamination in compression $(\sigma_{33} < 0)$:

$$\left(\frac{\sigma_{33}}{Z_C}\right)^2 + \left(\frac{\tau_{23}}{S_{23}}\right)^2 + \left(\frac{\tau_{13}}{S_{13}}\right)^2 \geq 1 \tag{7}$$

where $X_T, X_C, Y_T, Y_C, Z_T, Z_C$ are tensile and compressive strength in the 1,2 and 3 directions respectively. S_{12}, S_{13}, S_{23} are shear strengths.

Once a failure initiation criterion is satisfied, the damage evaluation model needs to be defined to simulate the progressive damage of composite materials. The corresponding exponential progressive damage evaluation law is taken into consideration in this paper, which evolves by calculating the damage variable (Guo et al., 2013). The continuous damage variable d_i is introduced. The subscripts i are ft, fc, mt, mc, dt, dc, representing the tensile and compression damage variables of the fibre, matrix and delamination, respectively. The expression is as follows:

Fibre tension failure $(\sigma_{11} > 0)$:

$$d_{ft} = 1 - \left(\frac{1}{e_{ft}}\right) e^{\left[-C_{11}\varepsilon_{11}^{ft}\varepsilon_{11}^{ft}\left(e_{ft}-1\right)L_C/G_{ft}\right]} \tag{8}$$

Fibre compression failure $(\sigma_{11} < 0)$:

$$d_{fc} = 1 - \left(\frac{1}{e_{fc}}\right) e^{\left[-C_{11}\varepsilon_{11}^{fc}\varepsilon_{11}^{fc}\left(e_{fc}-1\right)L_C/G_{fc}\right]} \tag{9}$$

Matrix tension failure $(\sigma_{22} > 0)$:

$$d_{mt} = 1 - \left(\frac{1}{e_{mt}}\right) e^{\left[-C_{22}\varepsilon_{22}^{mt}\varepsilon_{22}^{mt}\left(e_{mt}-1\right)/L_C/G_{mt}\right]} \tag{10}$$

Matrix compression failure $(\sigma_{22} < 0)$:

$$d_{mc} = 1 - \left(\frac{1}{e_{mc}}\right) e^{\left[-C_{22}\varepsilon_{22}^{mc}\varepsilon_{22}^{mc}\left(e_{mc}-1\right)L_C/G_{mc}\right]} \tag{11}$$

Fibre-Matrix shear out $(\sigma_{11} < 0)$:

$$G_{12}^{'} = 0, v_{12}^{'} = 0 \tag{12}$$

Delamination in tension $(\sigma_{33} > 0)$:

$$d_{dt} = 1 - \left(\frac{1}{e_{dt}} \right) e^{\left[-C_{33} \varepsilon_{33}^{dt} \varepsilon_{33}^{dt} (e_{dt} - 1) L_C / G_d \right]} \tag{13}$$

Delamination in compression $(\sigma_{33} < 0)$:

$$d_{dc} = 1 - \left(\frac{1}{e_{dc}} \right) e^{\left[-C_{33} \varepsilon_{33}^{dc} \varepsilon_{33}^{dc} (e_{dc} - 1) L_C / G_d \right]} \tag{14}$$

where the $G_{ft}, G_{fc}, G_{mt}, G_{mc}, G_{dt}$ is the corresponding fracture energy; L_C is the characteristic length of element; $G_{12}^{'}, v_{12}^{'}$ are damaged elastic properties and Poisson's ratio, respectively; $\varepsilon_{11}^{ft}, \varepsilon_{11}^{fc}, \varepsilon_{22}^{mt}, \varepsilon_{22}^{mc}, \varepsilon_{33}^{dt}, \varepsilon_{33}^{dc}$ are corresponding initial damage strain in the direction 1, 2 and 3 respectively. $\varepsilon_{11}^{ft} = \frac{X_T}{C_{11}^0}, \varepsilon_{11}^{fc} = \frac{X_C}{C_{11}^0}, \varepsilon_{22}^{mt} = \frac{Y_T}{C_{22}^0}, \varepsilon_{22}^{mc} = \frac{Y_C}{C_{22}^0},$ $\varepsilon_{33}^{dt} = \frac{Z_T}{C_{33}^0}, \varepsilon_{33}^{dc} = \frac{Z_C}{C_{33}^0}$, $C_{11}^0, C_{22}^0, C_{33}^0$ are initial stiffness matrix in the direction 1, 2 and 3 respectively. The calculation process is shown in Figure 1.

2.2 Cohesive zone model

The SLJs are made by bonding composite laminate with adhesives. Therefore, it is necessary to use suitable model to predict the failure of adhesive layer. The cohesive zone model (CZM) is used to simulate the damage initiation and evaluation of the adhesive layer in this study. The bilinear constitutive model of CZM is shown in Figure 2. In this paper, Quads (quadratic nominal stress criterion) criterion is used to judge the damage state of cohesive element, as shown in equation (15):

$$\left\{ \frac{t_n}{t_n^0} \right\}^2 + \left\{ \frac{t_s}{t_s^0} \right\}^2 + \left\{ \frac{t_t}{t_t^0} \right\}^2 = 1 \tag{15}$$

where t_n^0, t_s^0, t_t^0 are interfacial strengths corresponding to the onset of separation for each pure mode, respectively.

The ultimate failure displacement of cohesive element is defined by the fracture energy G^C and the fracture energy can be calculated by the Benzeggagh-Kenane fracture criterion (Benzeggagh and Kenane, 1996) expressed as:

$$G^C = G_n^C + \left(G_s^C - G_n^C \right) \left(\frac{G_s^C}{G_T} \right)^{\eta} \tag{16}$$

where G^C, G_n^C, G_s^C are the total, normal and shear critical fracture, respectively; G_S is the dissipated energy in the out-of-plane direction; G_T is the total dissipated energy in all three directions; The parameter η is related to material parameter. When the material is carbon fibre composite material, the parameter η takes 1~2. In this paper, η is set to 1.45, which is consistent with Sun et al. (2019).

Figure 1 The implementation of the SLJs numerical model showing schematically the overall flowchart for one each computational time-step (see online version for colours)

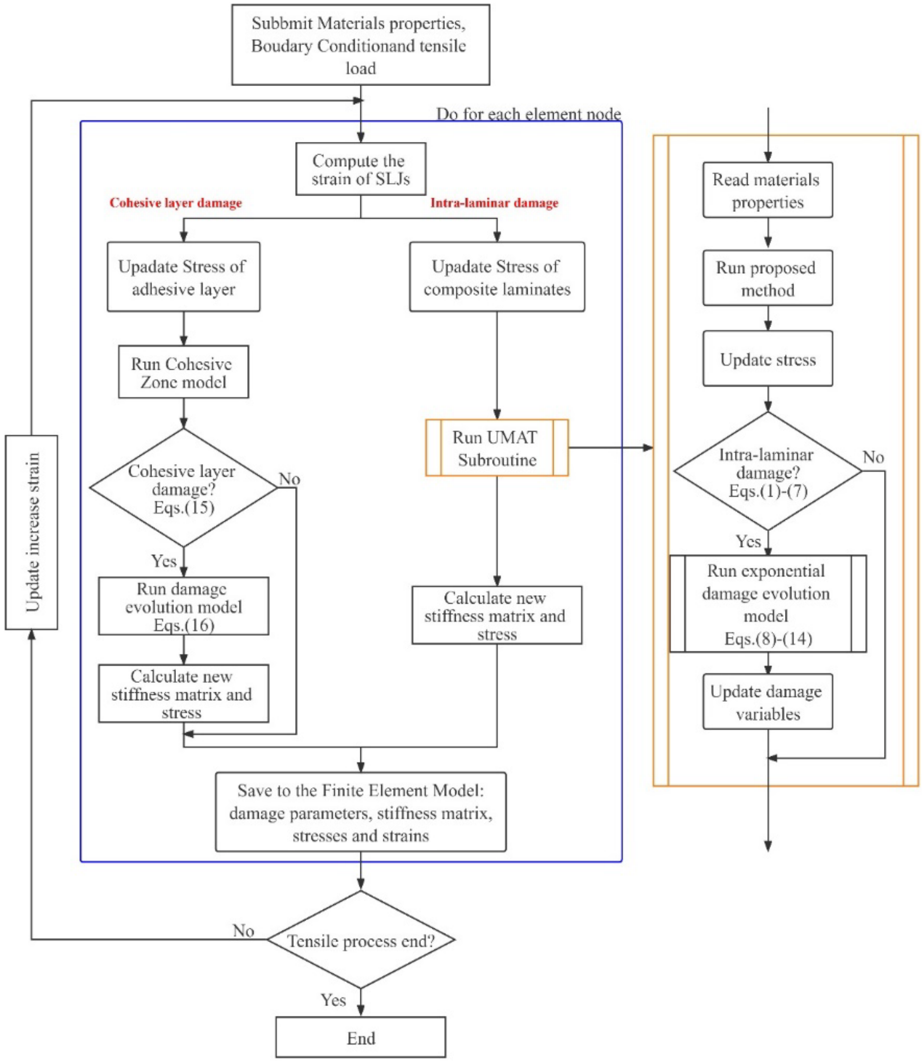

3 Validation of numerical model

The numerical analysis results are compared with the experimental results provided by Sun et al. (2019). The parameters of the verification model are shown in Figure 3. The total length of the SLJs is 200 mm. The overlap width and thickness of the composite laminate are 25 mm and 2.88 mm respectively. The thickness of cohesive layer is 0.2 mm. The stacking sequence of composite laminates is $\left[45^{\circ}/0^{\circ}/-45^{\circ}/90^{\circ}\right]_{3s}$. The 6 degrees of freedom (x, y, z) at the left end of the model are constrained. The right end is constrained except for the remaining 5 degrees of freedom and a displacement load along the x direction is applied. The FE model and boundary conditions are shown in Figure 4.

Figure 2 Cohesive zone model in mixed mode

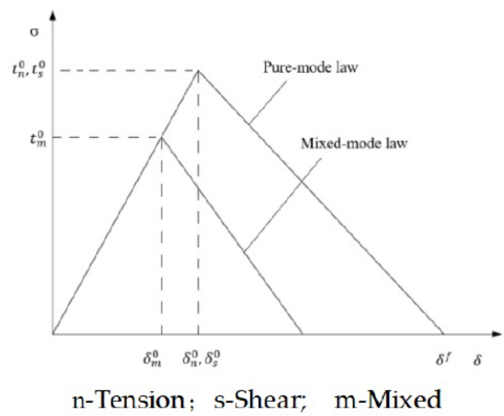

Figure 3 Finite element verification model of the adhesively bonded single-lap joints

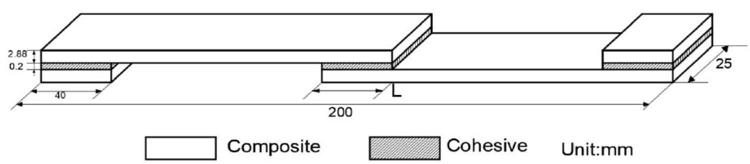

Figure 4 Boundary and loading conditions applied in FE models (see online version for colours)

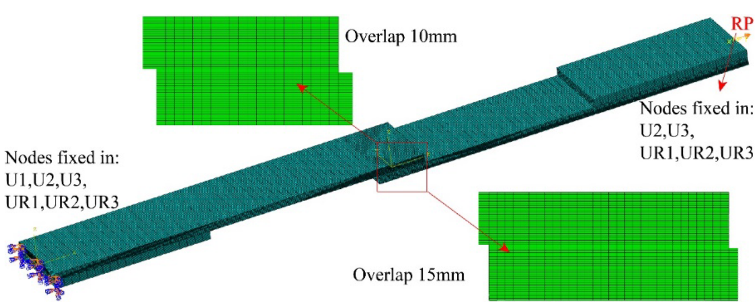

It is found that the FEM results are basically consistent with the experimental results, which have a similar overall trend. In terms of the ultimate failure load, the numerical results in this paper and the experimental results and numerical results have been shown in Table 1. The numerical results in this paper are roughly the same as the numerical results provided by Sun et al. (2019), which agree well with the experimental results. To sum up, the finite element model established in this paper can ensure the accuracy of the tensile performance of the SLJs and be accepted in engineering applications.

Table 1 Comparison of the FEM results in this study with experiment result and FEM result

	Overlap length 10 mm	*Overlap length 15 mm*	*Overlap length 10 mm error*	*Overlap length 15 mm error*
Experiment result/KN	4.20	6.13		
Simulation result in literature/KN	4.41	6.39	5.0%	4.3%
Simulation result in this study/KN	4.34	6.49	3.3%	5.9%

4 Simulation results and discussion

In order to study the SLJs with different parameters, the numerical models were established, as shown in Figure 5. Table 2 presents the mechanical properties of the T300/QY8911 unidirectional ply, which is provided by Sun et al. (2019). The adhesive layer thickness is 0.2 mm and the adhesive layer mechanical properties is shown in Table 3 (Sun et al. 2019). The dimensional parameters are shown in Table 4. The path A-B along the centre of the adhesive layer was established and the SDEG (damage variable of the adhesive layer), Von Mises, $s_{33}\left(\mathit{peel\ stress}\right)$ and $s_{13}\left(\mathit{shear\ stress}\right)$ were drawn. Where the s_{33} and s_{13} are responsible for cohesive failure.

Table 2 Mechanical properties of the unidirectional laminate

Density(kg/m³)	1600	
Engineering constant	Young's modulus (GPa)	$E_{11}=153; E_{22}=E_{33}=10.3$
	Poisson's ratio	$v_{12}=v_{13}=0.3; v_{23}=0.4$
	Shear modulus (GPa)	$G_{12}=G_{13}=6; G_{23}=3.70$
Strength properties (MPa)	Fibre tensile and compressive strength (MPa)	$X_T=2537; X_C=1580$
	Matrix tensile and compressive strength (MPa)	$Y_T=82; Y_C=236$
	Shear strength (MPa)	$S_{12}=S_{13}=90; S_{23}=40$
Fracture energy (N/mm)	Fibre tensile and compressive fracture Energy(N/mm)	$G_{ft}=91.6; G_{fc}=79.9$
	Matrix tensile and compressive fracture energy (N/mm)	$G_{mt}=0.22; G_{mc}=1.1$

Table 3 Material properties of cohesive elements

Elastic modulus (MPa)	$t_n=2210; t_s=t_t=780$
Strength properties (MPa)	$N=23.6; S=T=18.5$
Fracture energy (N/mm)	$G_n^C=1.1; G_s^C=G_t^C=2$

Figure 5 Design parameters of SLJs

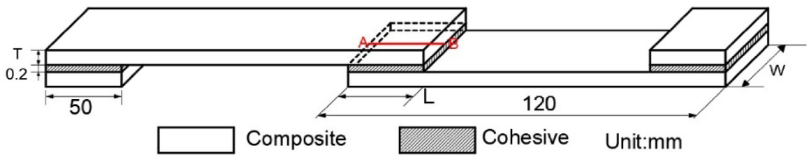

Table 4 Dimension parameters of the SLJs

Numerical analysis	*Lap length/mm*	*Lap width*	*Adherend thickness*	*Stacking sequence*
Influence of stacking sequences and overlap length	5 mm,10 mm, 15 mm,20 mm	25 mm	3.6 mm	$[45°/0°/–45°/90°]_{3s}$
			3.6 mm	$[45°/–45°]_{6s}$
			3.6 mm	$[0°/90°]_{6s}$
Influence of overlap width	15 mm	10 mm,15 mm, 20 mm,25 mm	3.6 mm	$\left[90^o / 45^o / 0^o / -45^o\right]_{3s}$
Influence of adherend thickness	15 mm	25 mm	1.2 mm	$\left[45^o / 90^o / 0^o / -45^o\right]_{s}$
			2.4 mm	$\left[45^o / 90^o / 0^o / -45^o\right]_{2s}$
			3.6 mm	$\left[45^o / 90^o / 0^o / -45^o\right]_{3s}$

4.1 Influence of stacking sequences and overlap length

The displacement-load curves of the SLJs under three stacking sequences are shown in Figure 6, which with different overlap lengths. In Figure 6, Label 1, Label2 and Label 3 represent the stacking sequences of $[45°/0°/–45°/90°]_{3s}$, $[45°/–45°]_{6s}$ and $[0°/90°]_{6s}$, respectively. For the same stacking sequence, the ultimate failure load and failure displacement of the SLJs increases with the increase of the overlap length. Under the same overlap length, the ultimate failure load of the SLJs is biggest with $[0°/90°]_{6s}$ and the ultimate failure load is smallest with $[45°/–45°]_{6s}$. The ultimate failure load of quasi-isotropic stacking sequence is located between $[45°/–45°]_{6s}$ and $[0°/90°]_{6s}$. The reason is that more 0^o plies used in $[0°/90°]_{6s}$ is beneficial for improving the tensile resistance of SLJs. It is found that the $[45°/–45°]_{6s}$ will maximise the failure displacement of the SLJs and the $[0°/90°]_{6s}$ will minimise failure displacement of SLJs. The reason for the phenomenon is that the addition of the 45^o and -45^o plies can enhance the shear resistance of the SLJs, but the tensile resistance of the SLJs will be weakened.

The SDEG and stress distribution along the path A-B at the point of peak force are drawn, as shown in Figures 7. In terms of peel stress (s_{33}), with the increase of the overlap length, the peel stress distribution trend changes from the ‘U’ to ‘M’ distribution, which indicates that the maximum peel stress position of the adhesive layer gradually moves from the edge to centre. The peel stress near the centre with stacking sequence of

[45°/–45°]$_{6s}$ is always higher than [45°/0°/–45°/90°]$_{3s}$ and [0°/90°]$_{6s}$. In some regions, the centre peel stress is negative, which is due to the rotation of the adhesive layer caused by the tensile load.

Figure 6 Displacement-load curves of the SLJs with different overlap lengths and stacking sequences (see online version for colours)

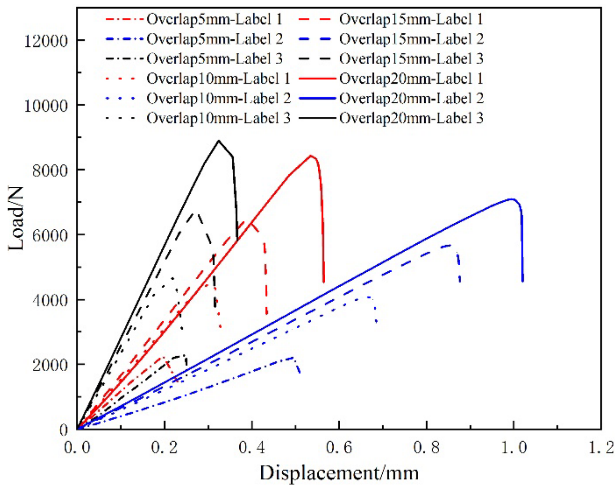

Figure 7 The distribution of S33-S13 (a) and SDEG-Von Mises (b) along the path A-B on the adhesive layer with a overlap length of 20 mm (see online version for colours)

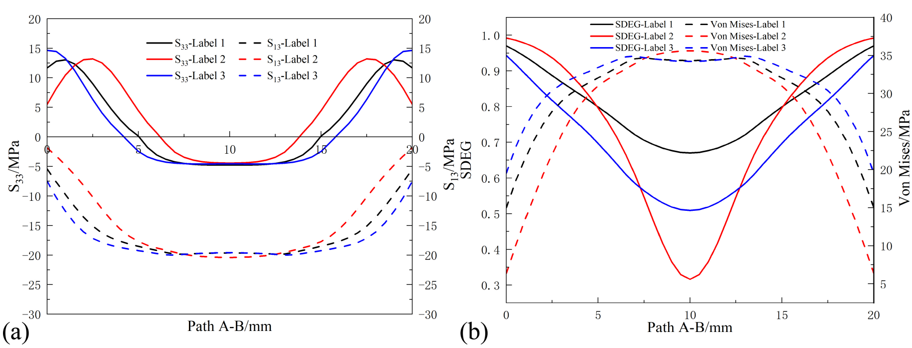

In terms of shear stress (s_{13}) distribution, with the increase of the overlap length, the distribution trend in the centre of adhesive layer is similar under the three stacking sequences. However, the s_{13} at the edge of cohesive layer gradually decreases. For tacking sequence of [45°/–45°]$_{6s}$, the s_{13} at the edge of cohesive layer is always at the lowest level. One phenomenon needs to be noticed that when the peel stress decreases, the shear stress increases.

The damage of each adhesive layer is shown in Figure 8. It can be found that, in the case of [45°/0°/–45°/90°]$_{3s}$, the undamaged center domain of the adhesive layer appears as a symmetrical drop. In the case of [45°/–45°]$_{6s}$, the undamaged center domain appears as an elliptical shape. In the case of [0°/90°]$_{6s}$, the undamaged center of the adhesive layer is distributed in a strip.

Figure 8 Adhesive layer damage under different overlap lengths and stacking sequences on the point of ultimate failure load (see online version for colours)

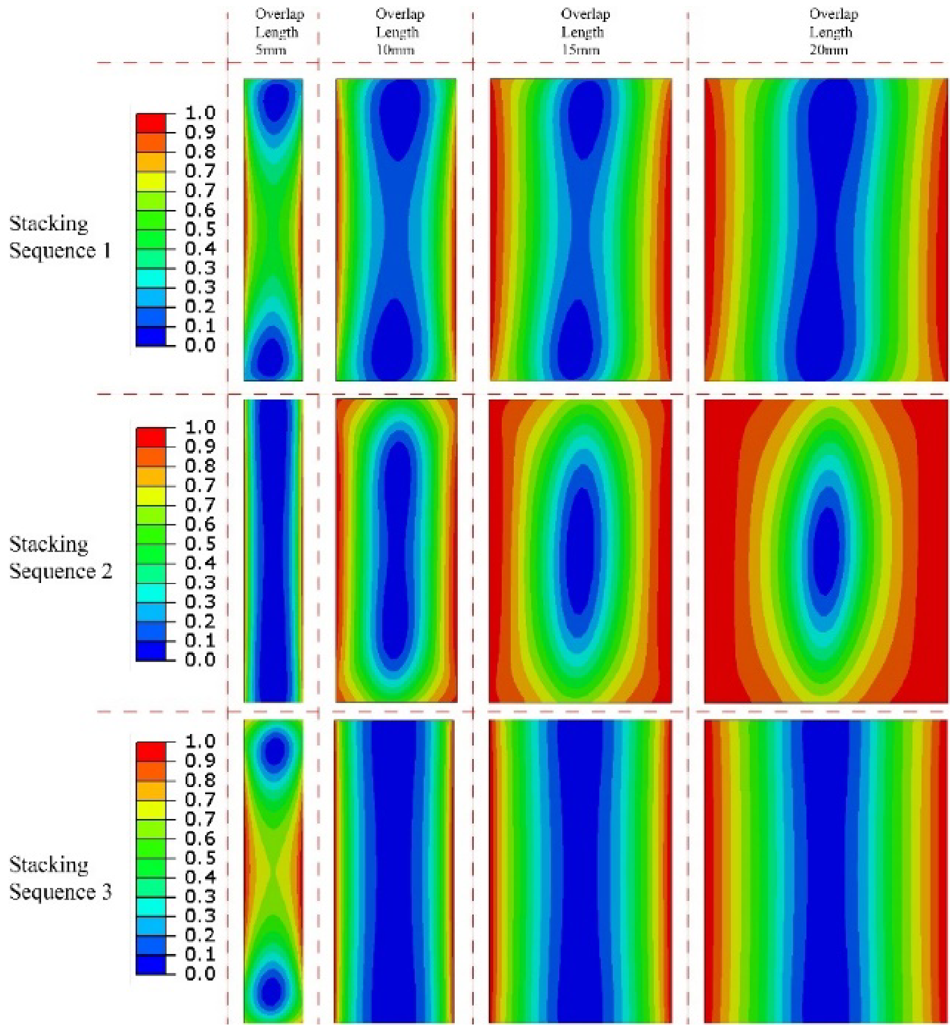

4.2 *Influence of overlap width*

The displacement-load curves of the SLJs with different overlap widths are shown in Figure 9. With the overlap width increasing, the ultimate failure load of the SLJs gradually increases. Compared with the ultimate failure load with overlap width of 10 mm, the failure load with 15 mm, 20 mm and 25 mm overlap width increased by 48.7%, 99.7% and 149.2% respectively. However, the failure displacements of the joints are 0.433 mm, 0.382 mm, 0.426 mm and 0.427 mm respectively, which are roughly equal.

Figure 9 Displacement-load curve of connectors with different overlap widths

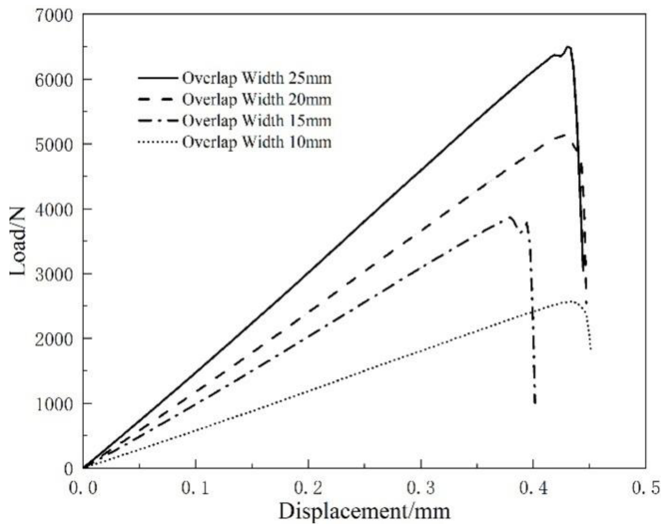

4.3 Influence of adherend thickness

Figure 10 shows the displacement-load curves of SLJs with three different thickness composite adherend. The ultimate failure load of the composite adherend with a thickness of 1.2 mm, 2.4 mm and 3.6 mm are 4.914 KN, 6.244 KN and 6.378 KN, respectively, which increase 27.15% and 29.79% compared with the 1.2 mm thickness adherend. It can be found that with linearly increasing of the adherend thickness, the ultimate failure load of the SLJs increases nonlinearly.

Figure 10 Displacement-load curve with different adherend thicknesses

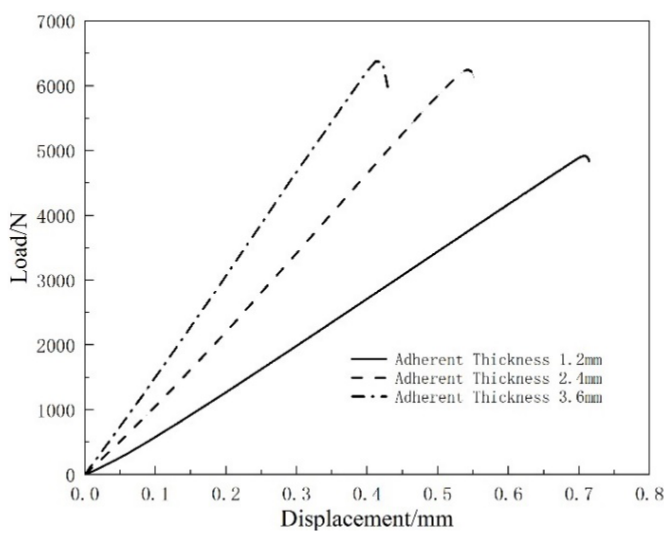

5 Conclusions

In this paper, a finite element model based on CDM is established to predict the connection performance and damage modes of the adhesively bonded single-lap joints (SLJs). Four design parameters including stacking sequences, overlap lengths, overlap widths and adherend thicknesses are analysed. The conclusions are as follows:

1. Although 0° and 90°° ply can improve the tensile performance of SLJs, it will also aggravate the damage of the adhesive layer, especially when the 90° ply adheres to the adhesive layer, there will be a variety of damage modes in the composite laminates; The ±45° plies in the composite laminate will relieve the adhesive layer damage, increase the failure displacement of the SLJs, and reduce the ultimate failure load of the SLJs.
2. With overlap length increasing, the edge of the adhesive layer is prone to fail and the stress distribution trend on the adhesive layer is closely affected by the 0° and 90° plies; With the overlap width increasing, however, there is no obvious change in the failure displacement, damage location and damage modes.
3. The damage modes of SLJs with different thicknesses of adherends are quite different. The damage of adherend with a small thickness is mainly matrix damage and delamination, accompanied by minor fibre damage; With of the thickness of adherend increasing, the matrix damage and delamination area decrease, however, the fibre damage area will increase; The composite laminates only show slight matrix damage at the edges with thicker composite adherend.

Acknowledgements

This work has been supported by the National Natural Science Foundation of China (11702046), Major Theme project of Chongqing Technology Innovation and Application Development (cstc2019jscx-zdztzx0028, cstc2019jscx-zdztzx0020).

References

Akderya, T., Kemiklioğlu, U. and Sayman, O. (2016) 'Effects of thermal ageing and impact loading on tensile properties of adhesively bonded fibre/Epoxy composite joints', *Compos. Part B-Eng.*, Vol. 95, pp.117–122.

Amiri, M. and Farahani, M. (2020) 'Adhesive composite joint reinforcement using button shape interlocking features', *Int. J. Adhes Adhes.*, Vol. 102, p.102651.

Barroso, A., Marín, J.C., Mantic, V. and París, F. (2020) 'Premature failures in standard test specimens with composite materials induced by stress singularities in adhesive joints', *Int. J. Adhes Adhes*, Vol. 97, pp.1–7.

Benzeggagh, M.L. and Kenane, K. (1996) 'Measurement of mixed-mode delamination fracture toughness of unidirectional glass/Epoxy composites with mixed-mode bending apparatus', *Compos. Sci. Technol.*, Vol. 56, pp.439–449.

Cheng, X.Q., Zhang, Q., Zhang, J. and Niu, Z. (2019) 'Parameter prediction of cohesive zone model for simulating composite/Adhesive delamination in hygrothermal enviorments', *Compos. Part B-Eng.*, Vol. 166, pp.710–721.

Cricrì, G. and Perrella, M. (2017) 'Investigation of mode III fracture behaviour in bonded pultruded GFRP composite joints', *Compos. Part B-Eng.*, Vol. 112, pp.176–184.

Daggumati, S., Sharma, A., Kasera, A. and Upadhyay, N. (2020) 'Failure analysis of unidirectional ceramic matrix composite lamina and cross-ply laminate under fiber direction uniaxial tensile load: cohesive zone modeling and brittle fracture mechanics approach', *J. of Materi. Eng. and Perform.*, Vol. 29, pp.2049–2060.

Demirala, M. and Kadioglu, F. (2018) 'Failure behaviour of the adhesive layer and angle ply composite adherends in single lap joints: a numerical study', *Int. J. Adhes. Adhes.*, Vol. 87, pp.181–190.

Felger, J., Stein, N., Frey, C. and Becker, W. (2019) 'Scaling laws for the adhesive composite butt joint strength derived by finite fracture mechanics', *Compos. Struct.*, Vol. 208, pp.546–556.

Floros, I. and Tserpes, K. (2019) 'Fatigue crack growth characterization in adhesive CFRP joints', *Compos. Struct.*, Vol. 207, pp.531–536.

Guo, W., Xue, P. and Yang, J. (2013) 'Nonlinear progressive damage model for composite laminates used for low velocity impact', *Appl. Math. Mech.-Engl.*, Vol. 34, pp.1145–1154.

Hashin, Z. (1980) 'Failure criteria for unidirectional fiber composites', *J. Appl. Mech.*, Vol. 47, pp.329–334.

Kim, M-H. and Hong, H-S. (2018) 'An adaptation of mixed-mode I+II continuum damage model for prediction of fracture characteristics in adhesively bonded joint', *Int. J. Adhes. Adhes.*, Vol. 80, pp.87–103.

Kupski, J., Teixeira de Freitas, S., Zarouchas, D., Camanho, pp. and Benedictus, R. (2019) 'Composite layup effect on the failure mechanism of single lap bonded joints', *Compos. Struct.*, Vol. 217, pp.14–26.

Masmanidis, I.T. and Philippidis, T.P. (2015) 'Progressive damage modeling of adhesively bonded lap joints', *Int. J. Adhes. Adhes.*, Vol. 59, pp.53–61.

Meng, L., Yang, X., Salcedo, E., Beak, D-C., Ryu, J.E., Zhe, L. and Zhang, J. (2020) 'A combined modeling and experimental study of tensile properties of additively manufactured polymeric composite materials', *J. of Materi. Eng. and Perform.*, Vol. 29, pp.2597–2604.

Orefice, A., Mancusi, G., Berardi, V.P., Feo, L. and Zuccaro, G. (2018) 'Residual stiffness of bonded joints for fiber-reinforced polymer profiles', *Compos. Part B-Eng.*, Vol. 144, pp.237–253.

Ribeiro, T.E.A., Campilho, R.D.S.G., da Silva, L.F.M. and Gogilo, L. (2016) 'Damage analysis of composite–aluminium adhesively-bonded single-lap joints', *Compos. Struct.*, Vol. 136, pp.25–33.

Sun, L.G., Li, C., Tie, Y., Hou, Y.L. and Duan, Y.C. (2019) 'Experimental and numerical investigations of adhesively bonded CFRP single-lap joints subjected to tensile loads', *Int. J. Adhes. Adhes.*, Vol. 95, p.102402.

Ungureanu, D., □ăranu, N., Lupă□teanu, V., Isopescu, D.N., Opri□an, G. and Mihai, P. (2018) 'Experimental and numerical investigation of adhesively bonded single lap and thick adherents joints between pultruded GFRP composite profiles', *Compos Part B-Eng*, Vol. 146, pp.49–56.

Ye, J.X., Yan, Y., Li, J., Hong, Y. and Tian, Z. (2018) '3D explicit finite element analysis of tensile failure behavior in adhesive-bonded composite single-lap joints', *Compos. Struct.*, Vol. 201, pp.261–275.

Yuan, Q.H., Yang, T., Yang, G.X., Liu, S.N., Du, Y. and Liu, C. (2019) 'Enhancing mechanical properties of adhesive laminates joints using ultrasonic vibration-assisted preprocessing', *Compos. Struct.*, Vol. 227, p.111325.